An optimized LQG servo controller design using LQI tracker for VSP-based AC/DC interconnected systems

Elyas Rakhshani [a], Iman Mohammad Hosseini Naveh [b], Hasan Mehrjerdi [c], Kaikai Pan [a,*]

[a] *Department of Electrical Sustainable Energy, Delft University of Technology, Delft, the Netherlands*
[b] *Department of Electrical Engineering, Gonabad Branch, Islamic Azad University, Gonabad, Iran*
[c] *Department of Electrical Engineering, Qatar University, Doha, Qatar*

ARTICLE INFO

ABSTRACT

This paper proposes a novel application for the optimal Linear Quadratic Gaussian (LQG) servo controller to enable a proper coordination of the AC/HVDC interconnected system with Virtual Synchronous Power (VSP) based inertia emulation. Particularly, the proposed control design takes the process disturbances and measurement noise of the studied VSP-HVDC system into account, while few studies have focused on this perspective. The proposed LQG controller with modifications is designed by means of a combination of Kalman Filter (state estimator) and an added Linear Quadratic Integrator (LQI) to observe the system model's states and track the reference commands while rejecting the effects of system noise. Besides, we utilize a swarm-based optimization algorithm to operate as the search process for the tuning of the elements in the weighting matrices involved in the controller design. The role of the proposed optimal LQG controller is to stabilize such AC/DC interconnected system with VSP-based inertia emulator while minimizing the associated performance index. According to the obtained simulation results, in addition to the advancement from the VSP-based approach for damping frequency oscillations excited by faults, application of the proposed LQG servo controller can achieve the targets on both estimating the state variables and tracking the reference signals with satisfactory performance, comparing with the conventional LQG regulator.

1. Introduction

Frequency control considering different approaches for enhancing its dynamic performance is the key to stability of modern power systems with low inertia [1–3]. Such systems are the results of phase out of conventional power plants, high penetration of renewable generations and increasing application of power electronic-based components [4–7]. The frequency response is much faster in these systems with low inertia, which makes the task of frequency control and system operation more challenging. Thus, considering the intermitted behavior in these renewable generation based systems, it is of utmost importance to develop an additional supplementary control loop for facilitating the fast frequency response capabilities of the power electronic-based generation units.

The recent research work has focused on synthetic inertia emulation and virtual synchronous generator (VSG) based strategies [8,9]. In general, virtual inertia emulation can be accomplished by using an advanced controller within the outer loop control of power converters. A short-term source of energy from the energy storage module is needed to enable an effective inertia emulation task. In this regard, many research activities have been carried out to propose different methods for mimicking the behavior of synchronous machines in the control loops of power converters [10–13]. According to these research reports, different methodologies are used to coordinate the power references of the electronic converters to provide synthetic inertia to the system. Using derivative control for emulating virtual inertia in HVDC-based systems is one of the major approaches at the system level [14–16]. To be noted, in most of the derivative and droop based approaches, the input signal for the inertia emulator is the frequency deviation. Usually, this inertia emulation approach based on the derivative term of the frequency is very sensitive to the noise of frequency measurements. Therefore, the confidence of these measurements has to be ensured in those methods. To overcome that, recent work has deployed techniques such as the Phase-Locked Loop (PLL) for a proper estimation of the measurement signals [17]. However, any amplified noise caused by frequency deviation measurements could still bring instability problems to the system.

This limitation can be even more problematic especially in the unsymmetrical systems or the system under abnormal faults.

Therefore, to explore better approaches of providing virtual inertia without the limitation of frequency signal measurements, our work in [18] proposed an alternative controller based on the VSP concept through the converter stations on the HVDC links in a multi-area AC/DC interconnected system. The dynamic effects of this virtual inertia emulation on system frequency dynamics are reflected in the multi-area automatic generation control (AGC) model. This control strategy has developed a new method for power converter control, behaving as a synchronous generator with the ability of virtual inertia emulation while the drawbacks of conventional generators are avoided [19]. Besides, from the main control loop of the VSP approach, we can derive a second-order characterization, which makes it possible to affect the system dynamics with both damping and inertia emulation concurrently for frequency control improvements.

Till now, we see that research work has been conducted on different virtual inertial emulation methods. However, to the best of our knowledge, in none of them a systematic advanced controller for suppressing the overall performance of the AC/DC system with VSP functionalities has been proposed. Besides, in the VSP approach for inertia emulation, to be more close to reality, one still needs to consider the presence noise in the system process and measurements and its effects on the system frequency dynamics. Therefore, significant research efforts are still needed to develop a suitable control approach which can provide better dynamics with proper coordination between the VSP station and the rest of the AC/DC system where there exist possible process disturbances and measurement noise.

In this paper, we aim to close this gap by proposing a new control strategy for the AC/DC interconnected system with VSP capabilities. The main objectives for modeling and controlling of this type of system are: (i) rejecting possible disturbances and noise which could appear in the practice of the VSP-HVDC system and affect system stability, while few studies have focused on this perspective; (ii) defining a suitable model with a global feedback law to enable a proper coordination between the VSP station and the rest of the AC/DC system for a stabilization and dynamic improvement of system dynamics. Therefore, to achieve these targets, the design of an optimal regulator for a novel application on the AC/DC interconnected system with VSP-based inertia emulation will be proposed. Linear quadratic regulator (LQR) could be a good option for this type of control applications [20]. However, the LQR law is based on the availability of full state variables which may not be completely measurable in most of the real-world situations. To overcome that, a Linear Quadratic Gaussian (LQG) servo controller is developed in this paper, using a Kalman Filter to estimate the full state vector of the VSP-HVDC system. Additionally, the conventional LQG regulator has no external input reference to track and still needs to be updated in a way

that the outputs (e.g., the frequency deviations) of the VSP-HVDC system converge to zero after contingencies. Thus we need a proper tracking of an introduced input command especially in the scenario where the system contains noise. Such noise might still lead to instability problems in the task of frequency control enabled by VSP for inertia emulation. To resolve this tracking issue, in this paper, a modification of the aforementioned LQG servo controller has been performed by incorporating the Kalman Filter (state estimator) with a Linear Quadratic Integrator (LQI). The LQI acts as a suitable full state feedback compensator and has the capability of increasing tracking error reduction for the global system, by rejecting the process and measurement noise.

To conclude, the contributions of this paper are reflected through the following aspects: (i) To the best of the authors' knowledge, it is the first study on proposing control strategy for the overall VSP-based AC/DC system, and a global feedback law enabling a proper coordination between the VSP station and the rest of the AC/DC system is proposed based on the concept of LQG; (ii) The LQG controller is modified to adapt to achieve the control goals on state estimation and reference tracking through a Kalman Filter and an added LQI module. Then the existence of noise in the studied VSP-HVDC system can be considered; (iii) Instead of using the typical trial-and-error method which is not effortless, we utilize a swarm-based optimization algorithm to operate as the search process for the tuning of the elements in the weighting matrices involved in the controller design.

In addition to the proposed LQG servo control structure, the effectiveness of the developed approach is also validated on a two-area VSP-based AC/DC system under abnormal faults and noise. The obtained simulation results from the proposed LQG servo controller illustrate that the VSP strategy can be effective in damping frequency oscillations excited by faults, and the proposed LQG controller can achieve the targets on both state estimation and reference tracking.

The outline of this paper is as follows. Section 2 presents the mathematical representation of the VSP-HVDC model, i.e., the two-area system with parallel AC/HVDC links and VSP capabilities. Our proposed LQG control structure and its design process is detailed explained in Section 3. Numerical results and discussions are reported in Sections 4 and the conclusion is draw in Section 5.

2. VSP-based AC/DC interconnected system

In this section, the VSP approach for inertia emulation through the converter stations of the HVDC links in a multi-area AC/DC interconnected system will be presented.
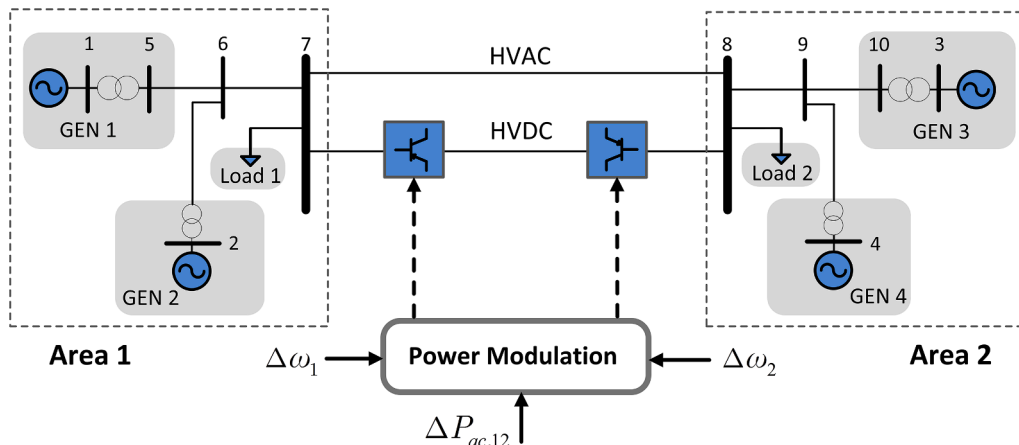

Fig. 1. The diagram of a two-area AC/DC interconnected system with VSP on the HVDC link.

2.1. Dynamic model of the VSP facilitated system

We deploy a high-level control architecture to simulate and analyse the frequency behavior of the multi-area system with parallel AC/HVDC lines and VSP capabilities. In general, the VSP approach is based on the control of voltage source converters through an active power synchronization loop and a virtual admittance [21]. After an analysis on the electromechanical model of the VSP, the dynamic relationship between input and output power of each converter station could be expressed as a second-order transfer function. Then, a characteristic equation of the VSP dynamic model can be derived for this second-order system, namely,

$$\ddot{y} + 2\zeta\omega_n\dot{y} + \omega_n^2 y = \omega_n^2 u_r, \tag{1}$$

where ζ is the damping factor and ω_n is the natural frequency. The input signal, u_r, is the reference DC power that is related to other states of the global multi-area system. The output signal consists of two states variables,

$$\Delta Y_{vsp} = \begin{bmatrix} \Delta X_{1,vsp} \\ \Delta X_{2,vsp} \end{bmatrix}. \tag{2}$$

where $\Delta X_{1,vsp}$ is the emulated power and $\Delta X_{2,vsp}$ denotes the derivative term of this power for each VSP. The unit of $\Delta X_{1,vsp}$ is in terms of Megawatt (MW). Based on the classic control concepts, this second-order system could be represented by a set of two linear state equations. Then this control process can be expressed as

$$\begin{bmatrix} \Delta\dot{X}_{1,vsp} & \Delta\dot{X}_{2,vsp} \end{bmatrix} = \begin{bmatrix} 0 & 1 \\ -\omega_n^2 & -2\zeta\omega_n \end{bmatrix} \begin{bmatrix} \Delta X_{1,vsp} \\ \Delta X_{2,vsp} \end{bmatrix} + \begin{bmatrix} 0 \\ -\omega_n^2 \end{bmatrix} \Delta U, \tag{3}$$

where ΔU denotes the input signal of the DC power reference ($\Delta P_{dc,ref}$) that is generated by other control signals; it will be detailed in what follows. Let us consider a two-area AC/DC interconnected system with Area i and Area k in Fig. 1. We can see that a VSP-based HVDC link is implemented between controlled areas. As the HVDC link is located between these two areas, the frequency deviation of each area is the most suitable control signal for ΔU. In case of parallel AC/DC lines, the AC tie-line power deviation could be used as another control signal to achieve suitable coordination between these two lines. Thus we have

$$\Delta U = K_{fi,vsp}\Delta\omega_i + K_{fk,vsp}\Delta\omega_k + K_{ac}\Delta P_{ac,ik}, \tag{4}$$

where $K_{fi,vsp}$, $K_{fk,vsp}$ and K_{ac} are the proportional coefficients for the frequency deviations $\Delta\omega_i$, $\Delta\omega_k$ and AC power flow deviations $\Delta P_{ac,ik}$ of these two areas, respectively. From the above description, it becomes clear that in Fig. 1, the signals of frequency deviations ($\Delta\omega_i$, $\Delta\omega_i$) in both areas and AC power deviation ($\Delta P_{ac,ik}$) are used to form the input signal ΔU of DC power reference in the power modulation center, with associated proportional coefficients in (4). Then the injected DC power deviations ($\Delta X_{1,vspi}$, $\Delta X_{1,vspk}$) on the HVDC line can be generated for both areas in the two-area system, using the second-order system expression in (3).

The state-space presentation in (3) will be part of the global model for the frequency dynamics of the two-area interconnected AC/DC system with VSP-based inertia emulation. For the frequency regulation, typically a low-order linearized model could be used to describe the load-generation dynamic behavior, namely the Automatic Generation Control (AGC) model. Thus to study the small signal modeling and stability of the high-level control structure, we can describe the frequency dynamics of these two AC/DC interconnected areas with a VSP-based HVDC link in the Laplace domain as the following equations,

$$\Delta\omega_i = \frac{K_{pi}}{1 + sT_{pi}} \left[\Delta P_{mi} - \Delta P_{li} - \Delta P_{ac,i} - \Delta X_{1,vspi} \right], \tag{5}$$

$$\Delta\omega_k = \frac{K_{pk}}{1 + sT_{pk}} \left[\Delta P_{mk} - \Delta P_{lk} - \Delta P_{ac,k} + \Delta X_{1,vspk} \right], \tag{6}$$

where ΔP_{mi}, ΔP_{mk} denote the total active power from all generation units (GENs) within Area i and Area k, separately. Taking the Area i as an instance, one can have $\Delta P_{mi} = \sum_{g=1}^{G_i} \Delta P_{mi,g}$ where G_i denotes the number of participated GENs, K_{pi} is the system gain and T_{pi} is the system time constant. The load variation is mentioned by ΔP_{li} and $\Delta P_{ac,i}$ is the AC power flow deviation for Area i. These variables can be further described by

$$\Delta P_{mi,g} = \frac{1}{1 + sT_{ch,ig}} \left[\frac{\Delta\omega_i}{R_{ig} \times 2\pi} - \phi_{ig}\Delta P_{agc,i} \right], \tag{7}$$

$$\Delta P_{ac,i} = \frac{T_{ik}}{s}[\Delta\omega_i - \Delta\omega_k], \quad \Delta P_{ac,k} = -\Delta P_{ac,i}. \tag{8}$$

In the equations above, R_{ig} denotes the droop of each generation unit in Area i, $T_{ch,ig}$ is the overall time constant of the turbine-governor model, $\Delta P_{agc,i}$ is the output signal from the secondary frequency control of AGC in Area i for power reference of each generation unit, and ϕ_{ig} is its area participating factor in the AGC operation (the summation of ϕ_{ig} in Area i would be equal to one), T_{ik} denotes the power coefficient of the AC line between Area i and k. The part of AGC control calculates the Area Control Error (ACE) of Area i. Now the ACE signal in the two-area system with the parallel AC/DC links needs to be adapted to contain the frequency deviations of that area and both AC/DC power flow deviations, and acts as the input for an integral control action,

$$ACE_i = \beta_i\Delta\omega_i + [\Delta P_{ac,i} + \Delta X_{1,vspi}], \tag{9}$$

$$ACE_k = \beta_k\Delta\omega_k + [\Delta P_{ac,k} - \Delta X_{1,vspk}], \tag{10}$$

$$\Delta P_{agc,i} = K_{ai}\frac{ACE_i}{s}, \tag{11}$$

$$\Delta P_{agc,k} = K_{ak}\frac{ACE_k}{s}, \tag{12}$$

where β_i and β_k denote the frequency bias in Area i and Area k, respectively, K_{ai} and K_{ak} represent the integral gain of the AGC controllers in these two areas.

In (5) and (6), the parts $\Delta X_{1,vspi}$ and $\Delta X_{1,vspk}$ denote the total output of the VSP-based HVDC link transmitted power. Thus for this one VSP station on the HVDC line in the two-area system, the following equations can be further derived from (3),

$$\Delta X_{1,vspi} = s\Delta X_{2,vspi}, \tag{13}$$

$$
\begin{aligned}
s\Delta X_{2,vspi} =\ & \left[\frac{K_{fi,vsp}\omega_{ni}^2}{2\pi} \right] \Delta\omega_i + \left[\frac{K_{fk,vsp}\omega_{ni}^2}{2\pi} \right] \Delta\omega_k \\
& + [K_{ac,vsp}\omega_{ni}^2]\Delta P_{ac,ik} - \omega_{ni}^2\Delta X_{1,vspi} \\
& - 2\zeta_i\omega_{ni}\Delta X_{2,vspi},
\end{aligned}
\tag{14}
$$

$$\Delta X_{1,vspk} = s\Delta X_{2,vspk}, \tag{15}$$

$$
\begin{aligned}
s\Delta X_{2,vspk} =\ & \left[\frac{K_{fi,vsp}\omega_{nk}^2}{2\pi} \right] \Delta\omega_i + \left[\frac{K_{fk,vsp}\omega_{nk}^2}{2\pi} \right] \Delta\omega_k \\
& + [K_{ac,vsp}\omega_{nk}^2]\Delta P_{ac,ik} - \omega_{nk}^2\Delta X_{1,vspk} \\
& - 2\zeta_k\omega_{nk}\Delta X_{2,vspk}.
\end{aligned}
\tag{16}
$$

To be noted, we use the AC tie-line power flow deviation as a control signal in the above explanation for the VSP-based DC link in order to achieve suitable coordination between these two lines; see (4). The coordinated AC line can be a parallel or any close line to the DC link. If
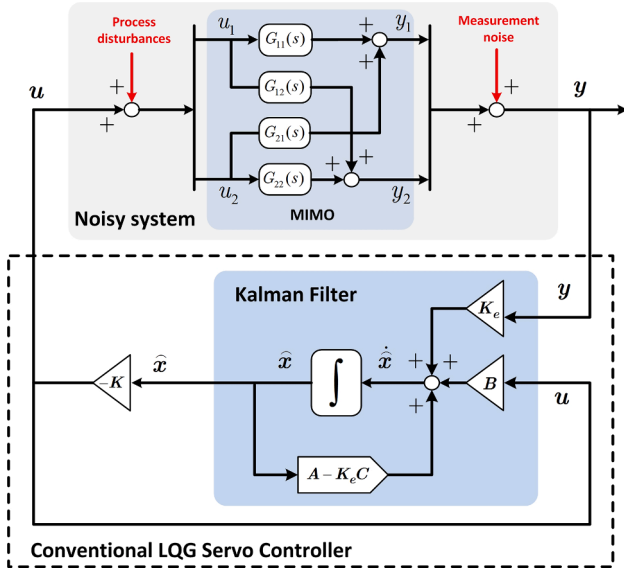
Fig. 2. Conventional structure of a LQG servo controller for the VSP-HVDC system considering noise.

there is just one DC link without a parallel AC line, this feedback signal will be zero and the rest of the model for the VSP-HVDC system will be the same. Besides, the model descriptions of this section can be generalized for a multi-area system with multiple VSP-based HVDC links [18].

Till this end, we can have a global linearized mathematical representation for the two-area AC/DC interconnected system with VSP-based inertia emulation, without considering the disturbances and noise, i.e., the VSP-HVDC model in the noiseless setting,

$$
\begin{cases} \dot{\boldsymbol{x}}(t) = \boldsymbol{A}\boldsymbol{x}(t) + \boldsymbol{B}\boldsymbol{u}(t), \\ \boldsymbol{y}(t) = \boldsymbol{C}\boldsymbol{x}(t), \end{cases} \tag{17}
$$

where $\boldsymbol{x} \in \mathbb{R}^{n_x}$ represents the vector of all state variables. In this model, there would be thirteen state variables ($n_x = 13$) such that

$$
\begin{aligned}
\boldsymbol{x} = [&\Delta\omega_1 \ \Delta\omega_2 \ \Delta P_{m1,1} \ \Delta P_{m1,2} \ \Delta P_{m2,1} \ \Delta P_{m2,2} \\
&\Delta P_{agc,1} \ \Delta P_{agc,2} \ \Delta P_{ac,12} \ \Delta X_{1,vsp1} \ \Delta X_{2,vsp1} \\
&\Delta X_{1,vsp2} \ \Delta X_{2,vsp2}]^\top.
\end{aligned} \tag{18}
$$

Note that $\Delta X_{1,vsp1}, \Delta X_{2,vsp1}, \Delta X_{1,vsp2}, \Delta X_{2,vsp2}$ are the four state variables of the two synchronous controllers for the VSP-based HVDC link. For the normal AC system without HVDC links, there would be no these states. In (17), the control inputs denoted by $\boldsymbol{u} \in \mathbb{R}^{n_u}$ are load variations in each area ($n_u = 2$); the measurable system outputs of $\boldsymbol{y} \in \mathbb{R}^{n_y}$ consist of frequencies in both areas ($n_y = 2$), i.e.,

$$
\boldsymbol{u} = [\Delta P_{l1} \ \Delta P_{l2}]^\top, \quad \boldsymbol{y} = [\Delta\omega_1 \ \Delta\omega_2]^\top. \tag{19}
$$

In addition, $\boldsymbol{A}$ is the state matrix, $\boldsymbol{B}$ is the control input gain matrix that relates the inputs to the system states, $\boldsymbol{C}$ is the output matrix, and all these matrices are with appropriate dimensions. The formulations of these matrices can be inferred from (5)–(16); here we omit the details. As we can see, the dynamic model (17) of the studied system with AC/DC interconnections and VSP-based inertia emulation can be represented as an multi-input multi-output (MIMO) system. Then the two inputs of load variations and the two outputs of frequencies from both areas in such MIMO system can be described by,

$$
\begin{bmatrix} y_1(s) \\ y_2(s) \end{bmatrix} = \begin{bmatrix} G_{11}(s) & G_{12}(s) \\ G_{21}(s) & G_{22}(s) \end{bmatrix} \begin{bmatrix} u_1(s) \\ u_2(s) \end{bmatrix}, \tag{20}
$$

$$
G_{vsp}(s) := \begin{bmatrix} G_{11}(s) & G_{12}(s) \\ G_{21}(s) & G_{22}(s) \end{bmatrix}. \tag{21}
$$

For implementation, from (21), $G_{vsp}(s)$ is applied as a MIMO transfer function in Laplace domain.

The frequency dynamics model in the form of (17) for the VSP-based AC/DC interconnected system has not considered process disturbances and measurement noise yet. In fact, the noise would still affect the implementations of the VSP-based virtual inertia emulation. Besides, as mentioned earlier, a control strategy is desired to enable better coordination between VSP stations and the rest of the AC/DC system in the presence of noise. Linear quadratic type of controller could be a good option for that purpose. One can consider Fig. 2 where we show the MIMO model for the VSP-HVDC system and a conventional LQG regulator to be designed. Both process disturbances and measurement noise are added in the studied system. As shown in Fig. 2, by combination control laws which are obtained from the noisy system and a Kalman Filter, the design process will be completed for a LQG regulator that is able to reject noise but has no external reference input to track. On the other hand, as a conventional regulation controller, the presented LQG structure in Fig. 2 still needs to be updated in a way that the output ($\boldsymbol{y}$ of frequency deviations) of the closed-loop VSP-HVDC system converges to zero after contingencies. In the following of Section 3, a modified LQG servo controller using an LQI tracker is proposed and designed. We introduce a reference signal such that the deviation of the output from the reference, which is called the tracking error, will then converge to zero. Notably in this end, Fig. 2 is presented also for achieving a common viewpoint and for a better understanding the relationship between the studied system and the controller to be designed: the MIMO model of VSP-HVDC system is described in Section 2, and the modified LQG controller is proposed in Section 3.

3. Proposed linear quadratic strategy in the presence of noise

To continue with Section 2, this section proposes our modified LQG servo controller design, based on a combination of a Kalman Filter and an LQI, for a new control strategy of the VSP-based AC/DC interconnected system. The main goal of the developed LQG controller is stabilization and dynamic improvement of the system under noise, by minimizing the magnitude of its associated performance index. In this section, we show how our proposed control strategy adapts to achieve the control goals: we start from the details of the conventional LQG regulator mentioned in Section 2 and move to the proposed LQG servo controller design, and further present a swarm–based algorithm to find the optimized values of the elements in the weighting matrices of the proposed controller.

3.1. Conventional LQG regulator

The LQG design problem is rooted in the optimal stochastic control theory and has many real-world applications. The LQG controllers are built for uncertain linear systems disturbed by additive white Gaussian noise and equipped with incomplete state information. It combines both concepts of Liner Quadratic Regulators (LQR) for full state feedback and Kalman Filter for state estimation. Considering the additive terms of disturbances and noise in practice, the state-space model of the VSP-HVDC system presented in (17) can be extended to the following equation in the noisy setting,

$$
\begin{cases} \dot{\boldsymbol{x}}(t) = \boldsymbol{A}\boldsymbol{x}(t) + \boldsymbol{B}\boldsymbol{u}(t) + \boldsymbol{G}\boldsymbol{w}(t), \\ \boldsymbol{y}(t) = \boldsymbol{C}\boldsymbol{x}(t) + \boldsymbol{v}(t), \end{cases} \tag{22}
$$

where $\boldsymbol{w} \in \mathbb{R}^{n_w}$ and $\boldsymbol{v} \in \mathbb{R}^{n_v}$ denote the stochastic disturbances and noise associated with the system process and the measurements, respectively. The matrix $\boldsymbol{G}$ (plant noise gain matrix) is also constant with an appropriate dimension in the LTI (linear time-invariant) system. In this paper, we say that $\boldsymbol{w}$ and $\boldsymbol{v}$ are independent (uncorrelated) white Gaussian noises, satisfying,

$$E(\boldsymbol{w}) = E(\boldsymbol{v}) = \boldsymbol{0}, \ E(\boldsymbol{w}\boldsymbol{w}^\top) = \boldsymbol{W}, \ E(\boldsymbol{v}\boldsymbol{v}^\top) = \boldsymbol{V}. \tag{23}$$

As mentioned earlier, by attention to (23), $\boldsymbol{w}$ and $\boldsymbol{v}$ are assumed to be white Gaussian noise with zero means. Besides, they have covariance matrices of $\boldsymbol{W}$ and $\boldsymbol{V}$. It is assumed that $\boldsymbol{w}$ and $\boldsymbol{v}$ are uncorrelated in order to simply many expressions and derivations.

In real-world control design problems, it is rarely possible to have access to all of the system states which are needed for full state feedback. Instead, it is only possible to access some specific measurable system outputs. If these measurements carry enough information about the system states, then a state observer using Kalman Filter could be implemented to estimate all the system states. The Kalman Filter (state estimator) is a mathematical powerful tool that implements a predictor–corrector type estimator. This observer is capable of rejecting system process disturbances and measurement noise by acting as a low-pass filter. The main inputs to the Kalman state estimator are the control input $\boldsymbol{u}$ and the system output $\boldsymbol{y}$ in (22). Then, the state-space equations of the Kalman state estimator can be described by

$$\begin{cases} \dot{\widehat{\boldsymbol{x}}}(t) = (\boldsymbol{A} - \boldsymbol{K}_e)\widehat{\boldsymbol{x}}(t) + \boldsymbol{B}\boldsymbol{u}(t) + \boldsymbol{K}_e\boldsymbol{y}(t), \\ \widehat{\boldsymbol{y}}(t) = \boldsymbol{C}\widehat{\boldsymbol{x}}(t), \end{cases} \tag{24}$$

where $\widehat{\boldsymbol{x}}$ and $\widehat{\boldsymbol{y}}$ are the estimated states and outputs, $\boldsymbol{K}_e$ is the Kalman Filter gain. It should be mentioned that the matrices $\boldsymbol{A}, \boldsymbol{B}$ and $\boldsymbol{C}$ in (24) are the same as the ones in the system model (22). By a simplification of (24), we can achieve the following dynamic form for the Kalman estimator as well,

$$\dot{\widehat{\boldsymbol{x}}}(t) = \boldsymbol{A}\widehat{\boldsymbol{x}}(t) + \boldsymbol{B}\boldsymbol{u}(t) + \boldsymbol{K}_e(\boldsymbol{y}(t) - \widehat{\boldsymbol{y}}(t)). \tag{25}$$

In Fig. 2, the conventional structure of a LQG regulator for the VSP-HVDC system represented by an MIMO model has been depicted. We can see that a typical LQG controller is formed by connecting the system and the Kalman Filter through the optimal state estimation gain $\boldsymbol{K}_e$. Then it creates full state feedback by using the estimated states $\widehat{\boldsymbol{x}}$ which would pass through the optimal feedback gain $\boldsymbol{K}$. Because of the stochastic separation principle, the previously mentioned gains could be designed individually [22].

The conventional design process of a LQG controller starts with the calculation of the optimal state estimation gain $\boldsymbol{K}_e$, which will be illustrated in (26). Here $\boldsymbol{P}_e$ is a positive semi-definite matrix and the unique solution of the filter algebraic Riccati equation [23]. This solution ensures a minimum value of the performance index $\boldsymbol{J}_e$ for the steady-state error covariance as noted in (26).

$$\begin{cases} \boldsymbol{J}_e = \lim_{t \to \infty} E((\boldsymbol{x} - \widehat{\boldsymbol{x}})(\boldsymbol{x} - \widehat{\boldsymbol{x}})^\top), \\ \boldsymbol{A}\boldsymbol{P}_e + \boldsymbol{P}_e\boldsymbol{A}^\top + \boldsymbol{G}\boldsymbol{W}\boldsymbol{G}^\top - \boldsymbol{P}_e\boldsymbol{C}^\top\boldsymbol{V}^{-1}\boldsymbol{C}\boldsymbol{P}_e = \boldsymbol{0}, \\ \boldsymbol{K}_e = \boldsymbol{P}_e\boldsymbol{C}^\top\boldsymbol{V}^{-1}. \end{cases} \tag{26}$$

Besides, in the above description, to be mentioned, $\boldsymbol{W}$ and $\boldsymbol{V}$ introduced in (23) are symmetric positive definite matrices.

Next, the design of a typical LQG controller continues to compute the optimal state feedback gain $\boldsymbol{K}$, for which the state feedback law minimizes the quadratic cost function $\boldsymbol{J}_k$ which is described in the following Eq. (27). The resulted solution $\boldsymbol{P}_k$ is a positive semi-definite matrix and the solution of the control algebraic Riccati equation. Similarly, this solution ensures a minimum value of the performance index $\boldsymbol{J}_k$ in the quadratic form.

$$\begin{cases} \boldsymbol{J}_k = \lim_{T \to \infty} \left(\int_0^T (\boldsymbol{x}^\top\boldsymbol{Q}_k\boldsymbol{x} + \boldsymbol{u}^\top\boldsymbol{R}_k\boldsymbol{u})dt \right), \\ \boldsymbol{A}^\top\boldsymbol{P}_k + \boldsymbol{P}_k\boldsymbol{A} + \boldsymbol{Q}_k - \boldsymbol{P}_k\boldsymbol{B}\boldsymbol{R}^{-1}\boldsymbol{B}^\top\boldsymbol{P}_k = \boldsymbol{0}, \\ \boldsymbol{K} = \boldsymbol{R}_k^{-1}\boldsymbol{B}^\top\boldsymbol{P}_k. \end{cases} \tag{27}$$

Unlike the filter algebraic Riccati equation in (26) which only requires noise covariance matrices $\boldsymbol{W}$ and $\boldsymbol{V}$, we can see that the control algebraic Riccati equation in (27) requires two weighting matrices:
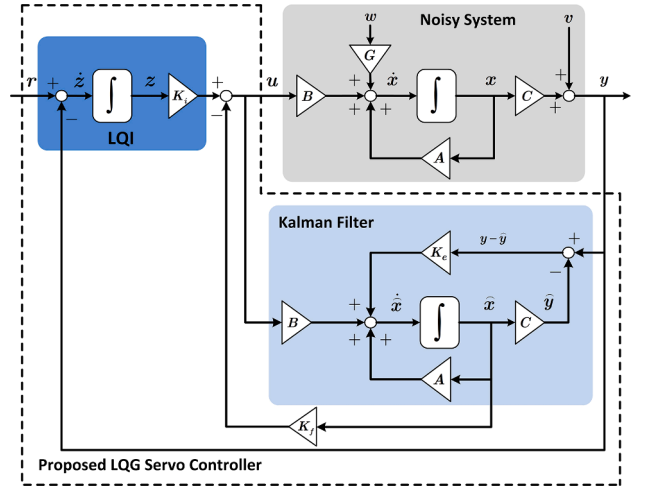
Fig. 3. Modified LQI scheme for the LQG servo controller.

(i) $\boldsymbol{Q}_k$ will be a symmetric positive semi-definite matrix;
(ii) $\boldsymbol{R}_k$ will be a symmetric positive definite matrix.

These weighting matrices provide a means to trade off two opposing objectives: regulation performance and control effort. Normally, they could be selected based on the trial-and-error approach. After the calculation of the optimal gains, the overall closed-loop system could be created by augmenting the noisy VSP-HVDC system with the Kalman Filter, resulting in the system model as illustrated in Fig. 2.

3.2. The proposed LQG servo controller using LQI tracker

In Section 3.1, a conventional LQG controller is designed by using the optimal state estimator (Kalman Filter) and the full state feedback strategy. In this section, in order to ensure an appropriate reference signal pursuit on the control system, we add an integrator with a separate gain to the proposed LQG control. The structure of the developed LQG controller achieved by an LQI is shown in Fig. 3.

For the proposed LQG controller, the Kalman Filter gain matrix can be obtained using the same approach in (26) which is initially for the conventional LQG, while the optimal feedback gain has been modified that it is now defined by matrices $\boldsymbol{K}_i$ and $\boldsymbol{K}_f$. To include the dynamics of the integral action into the state-space Eq. (22) and calculate the matrices $\boldsymbol{K}_i$ and $\boldsymbol{K}_f$ for the optimal gain, the tracking error named z is added as shown in Fig. 3, and is be defined by

$$\dot{\boldsymbol{z}}(t) = \boldsymbol{r}(t) - \boldsymbol{y}(t), \tag{28}$$

where $\boldsymbol{r}$ is the reference signal (note that in the conventional LQG of Fig. 2, there is no such reference signal to track) and $\dot{\boldsymbol{z}}$ before the integral action represents the difference between the measured system output and the reference command. To conclude here, the proposed LQG controller mainly contains a Kalman Filter for full state estimation and an LQI for reference tracking, as shown in Fig. 3. For the Kalman Filter, we can see from Eqs. (24) and (25) that the inputs to Kalman Filter are $\boldsymbol{y}$ and $\boldsymbol{u}$ of the VSP-HVDC system, i.e., the measurements of frequency deviations and the load variations inputs to the system; the outputs of the Kalman Filter are the estimated state variables $\widehat{\boldsymbol{x}}$. For the LQI tracker, its inputs are $\boldsymbol{y}$ and the reference signal $\boldsymbol{r}$, while its outputs together with the outputs of the Kalman Filter are associated with respective gains to be returned to the system; we provide the details of the controller design in the following. Firstly, by replacing $\boldsymbol{y}(t)$ with the expression in (22), we can further obtain the following equation,

$$\dot{\boldsymbol{z}}(t) = \boldsymbol{r}(t) - \boldsymbol{C}\boldsymbol{x}(t) - \boldsymbol{v}(t). \tag{29}$$

Therefore, to study the dynamic behavior of the whole closed-loop

system, one can argument the state of the plant in (22) together with $z(\cdot)$, yielding,

$$\begin{cases} \begin{bmatrix} \dot{x}(t) \\ \dot{z}(t) \end{bmatrix} = A_z \begin{bmatrix} x(t) \\ z(t) \end{bmatrix} + B_z \begin{bmatrix} u(t) \\ r(t) \end{bmatrix} + \begin{bmatrix} G & 0 \\ 0 & -I \end{bmatrix} \begin{bmatrix} w(t) \\ v(t) \end{bmatrix}, \\ y(t) = C_z \begin{bmatrix} x(t) \\ z(t) \end{bmatrix} + \begin{bmatrix} 0 & I \end{bmatrix} \begin{bmatrix} w(t) \\ v(t) \end{bmatrix}, \end{cases} \quad (30)$$

where the involved matrices can be expressed as

$$A_z = \begin{bmatrix} A_{(n_x \times n_x)} & 0_{(n_x \times n_y)} \\ -C_{(n_y \times n_x)} & 0_{(n_y \times n_y)} \end{bmatrix},$$
$$B_z = \begin{bmatrix} B_{(n_x \times n_u)} & 0_{(n_x \times n_y)} \\ 0_{(n_y \times n_u)} & I_{(n_y \times n_y)} \end{bmatrix},$$
$$C_z = \begin{bmatrix} C_{(n_y \times n_x)} & 0_{(n_y \times n_y)} \end{bmatrix}.$$

Recall that n^x, n^y and n^u denote the numbers of VSP-HVDC system states, measured outputs and input variables of load changes, and $n^x = 13, n^y = 2$ and $n^u = 2$ in the VSP-HVDC model, according to Section 2. Besides, we can also have

$$u(t) = K_i z(t) - K_f \widehat{x}(t) = \begin{bmatrix} -K_f & K_i \end{bmatrix} \begin{bmatrix} \widehat{x}(t) \\ z(t) \end{bmatrix}. \quad (31)$$

Then, by attention to the preceding and the difference between Figs. 2 and 3, the optimal state-feedback matrix in the proposed LQG controller by an LQI in Fig. 3 will include two separated parts as follows: $K = \begin{bmatrix} -K_f & K_i \end{bmatrix}$. With a similar treatment, this optimal state-feedback matrix can be computed from (27) by replacing the matrices A and B with A_z and B_z, respectively.

In the typical LQG design, one needs to test with different weighting matrices (i.e., Q_k and R_k in (27)) so that the performance and robustness requirements are achieved. The parameters of the weighting matrices are usually adjusted manually by the trial-and-error method which is not effortless in practice. In the following subsection, we present a swarm–based algorithm to find the optimized values of the elements in the weighting matrices.

3.3. LQG servo–controller tuning by GWO

From the above mentioned LQG design procedure, it is necessary to select the two weighting matrices (Q_k, R_k) in order to solve the algebraic Riccati equations and then obtain the gain matrix K, in (27). There is an infinite number for the selection of these two weighting matrices. The trial-and-error method is typically used, while here we utilize a swarm–based optimization algorithm for a more efficient computation and a more accurate solution.

We utilize a new meta-heuristic called Grey Wolf Optimizer (GWO). The GWO appears to be a well-regarded swarm intelligence optimization algorith. The main part of swarm–based algorithm in GWO imitates by the social interconnection (leadership hierarchy and hunting mechanism) of grey wolves in nature. The steps involved in the GWO algorithm and the mathematical descriptions are referred to the pioneering work [24].

By attention to the determined features of step response and its accessibility in every iteration of simulation, different fitness functions need to be used for that purpose. In this work, three performance indices are considered: Integral of Absolute Error (IAE), Integral of Time multiplied by Absolute Error (ITAE) and Integral of Time multiplied by the Squared Error (ITSE). These performance indices (cost functions) are defined by the following Eq. (32) where frequency deviations in Area 1 and Area 2 ($\Delta\omega_1$ and $\Delta\omega_2$) also tie-line AC power deviation between these two areas ($\Delta P_{ac,12}$) will be calculated in the time domain.
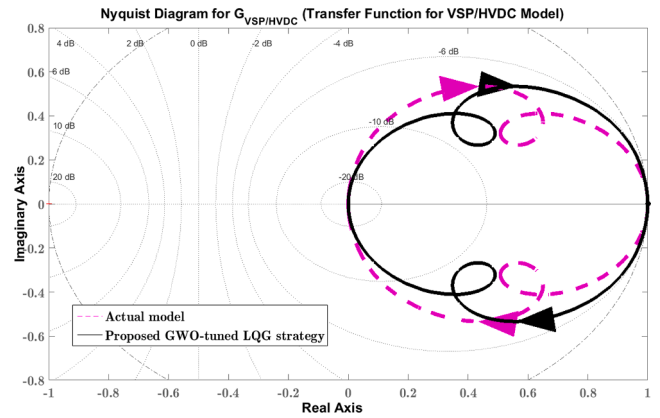

Fig. 4. Nyquist diagram for the transfer function $G_{vsp}(s)$ of the VSP–HVDC model.

$$J_{IAE} = \int_0^{T_f} |\Delta\omega_1 + \Delta\omega_2 + \Delta P_{ac,12}| dt,$$
$$J_{ITAE} = \int_0^{T_f} t |\Delta\omega_1 + \Delta\omega_2 + \Delta P_{ac,12}| dt, \quad (32)$$
$$J_{ITSE} = \int_0^{T_f} t \left(\Delta\omega_1^2 + \Delta\omega_2^2 + \Delta P_{ac,12}^2 \right) dt,$$

where T_f is the final simulation time. In the end, the following process illustrates the steps involved in the proposed algorithm achieved by GWO for the tuning of the optimized values of the elements in the weighting matrices:

1) Set up initial parameters for GWO;
2) Calculate the state-feedback gain based on (27);
3) Extract the frequency and AC power flow deviations ($\Delta\omega_1$, $\Delta\omega_2$ and $\Delta P_{ac,12}$);
4) Calculate the fitness values based on (32);
5) Check if the last iteration reaches: if yes, update GWO parameters and continue from the step of 2); otherwise, derive and display the optimized values.

4. Numerical results

In this section, in order to evaluate the performance of the proposed LQG servo controller for the novel application on the VSP-HVDC system in the presence of noise, different simulations are performed on the two-area AC/DC interconnected system with VSP functionalities. The simulations are done using the Matlab platform. In all of the simulations, the abnormal faults are considered as step load changes in Area 1. This is implemented based on the following equation,

$$\Delta P_{l1} = \begin{cases} 0.03 & 2 \leqslant t < 30, \\ 0.015 & t \geqslant 30, \\ 0 & \text{otherwise}, \end{cases} \quad (33)$$

where the values are all in per-unit. It is assumed that contingencies/faults happened as step load changes in Area 1 by increasing 0.03p.u. at $t = 2$s, and then the step load change becomes 0.015p.u. at $t = 30$s. The values of the two-area system parameters and also the parameters for the VSP parts in the state-space model (17) are referred to [14,21].

We highlight that the load deviations in the two areas ($\Delta P_{l1}, \Delta P_{l2}$) are presented as the input variables. In addition, the measured outputs in this process are considered as the frequency deviations ($\Delta\omega_1, \Delta\omega_2$) in both areas. Therefore, the nature of the process disturbance, as the input noise, is assumed to be the abnormal load changes in each area. Besides, the measurement noise can be observed in the output side of studied VSP-HVDC system model. The source of the measurement noise in real-

Table 1
Variation of the cost functions versus iteration.

Iteration	IAE	ITAE	ITSE
50	0.008607	7.514	12.35
100	0.008507	7.014	0.8084
150	0.000226	2.039	0.01286
200	0.000126	1.1278	0.00286
250	0.000052	1.0086	0.00108

world applications comes from the sensing process and some unexpected changes during the data transmission in the communication channels. Till this end, it is noteworthy again that the applied noise is considered as the white Gaussian noise with zero mean in our numerical simulation results of this paper.

4.1. System analysis: Nyquist's stability criterion

To begin with, we provide the Nyquist analysis of the whole closed-loop VSP-HVDC model in Fig. 4. The stability criterion of Nyquist is a graphical technique for determining the stability of a dynamical system. It relates the stability of a closed-loop system to the open-loop frequency response and open-loop pole location. The Nyquist technique is limited to linear, time-invariant (LTI) systems and has been widely used for designing and analyzing systems with feedback control loops. A practical advantage of the technique is that it can be applied directly to measured frequency response data. As we know, the system in a closed-loop configuration is stable if and only if the trajectory of the Nyquist diagram of $G(j\omega)H(j\omega)$ from $-\infty < \omega < \infty$ surrounds the point $(-1, 0)$ in a counter-clockwise direction as much times as the number of unstable poles that $G(s)H(s)$ has. This definition can be achieved by the generalized stability criterion of Nyquist for an MIMO system, which is an adaptation from the stability criterion for SISO (single-input single-
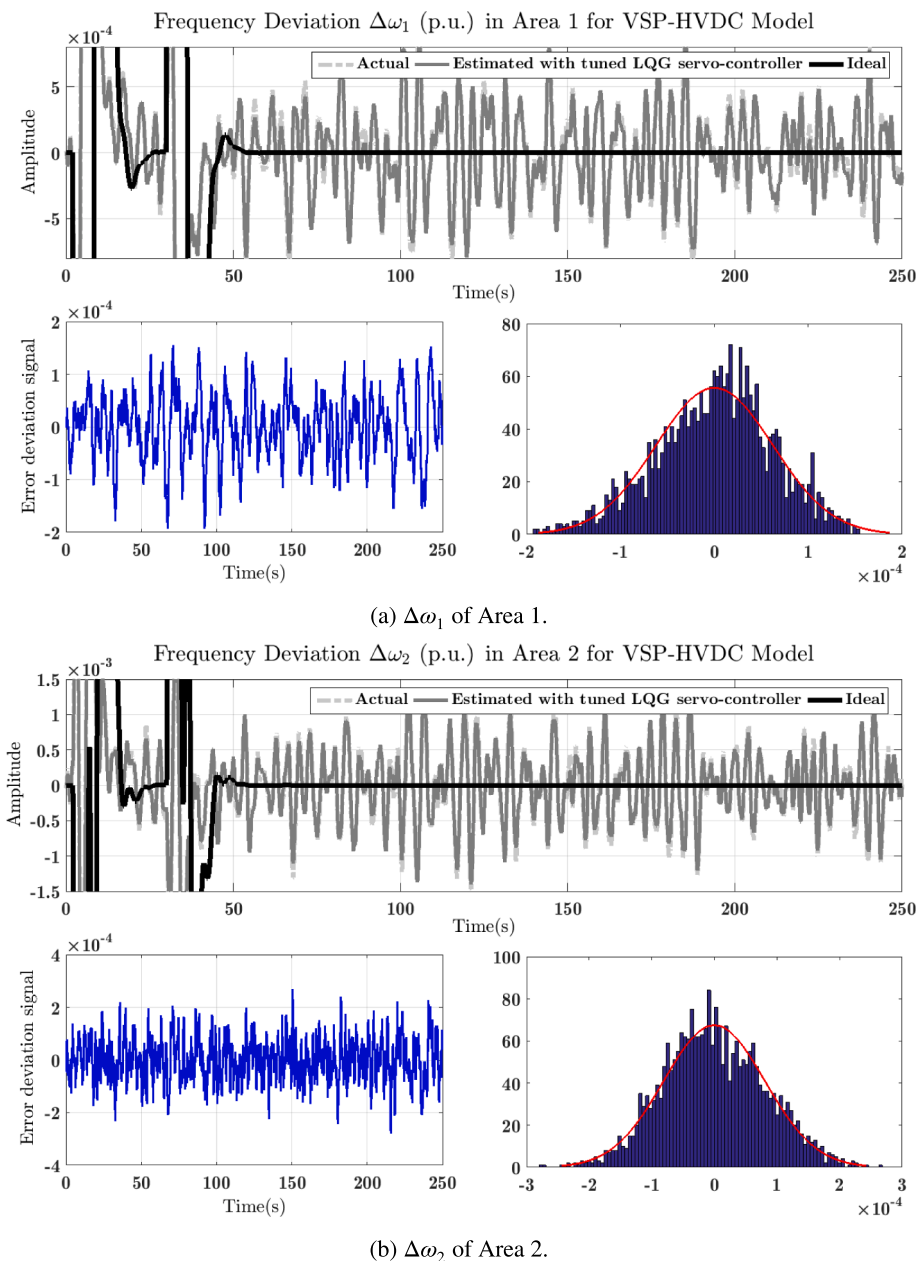

(a) $\Delta\omega_1$ of Area 1.

(b) $\Delta\omega_2$ of Area 2.

Fig. 5. Variation of actual and estimated frequency deviations using the proposed LQG controller tuned by the GWO algorithm. "Actual" corresponds to the MIMO system considering noise; "Ideal" corresponds to the system without considering any noise.

Table 2
Digitized results of $\Delta\omega_1$ in Fig. 5.

Time(s)	Actual	Estimated	Error deviation
10	1.830×10^{-3}	1.822×10^{-3}	8×10^{-6}
50	-1.861×10^{-4}	-1.418×10^{-4}	-4.43×10^{-5}
100	2.665×10^{-4}	2.326×10^{-4}	3.39×10^{-5}
150	2.518×10^{-4}	1.714×10^{-4}	8.04×10^{-5}
200	4.462×10^{-4}	3.903×10^{-4}	5.59×10^{-5}
250	-1.817×10^{-4}	-1.475×10^{-4}	-3.42×10^{-5}

Table 3
Digitized results of $\Delta\omega_2$ in Fig. 5.

Time(s)	Actual	Estimated	Error deviation
10	2.2383×10^{-4}	2.436×10^{-4}	-5.30×10^{-6}
50	3.455×10^{-4}	4.031×10^{-4}	-5.76×10^{-5}
100	-6.247×10^{-4}	-6.364×10^{-4}	1.17×10^{-5}
150	5.267×10^{-5}	-3.368×10^{-5}	8.635×10^{-5}
200	-8.234×10^{-5}	-3.047×10^{-4}	2.223×10^{-4}
250	-1.689×10^{-4}	-1.789×10^{-4}	1.00×10^{-5}

output) systems [25,26]. By attention to Section 2 and the continuous-time model descriptions in (17), a transfer function has been defined as $G_{vsp}(s)$ in Eq. (21) for the studied VSP-HVDC model.

4.2.2. Simulation results of the estimation target

As show in Fig. 3 of Section 3, the proposed LQG servo controller using an LQI tracker contains two stages. The first stage uses a Kalman

$$K_f = 10^{-3} \times \begin{bmatrix} -0.1187 & -0.0410 & -0.0089 & -0.0089 & -0.0855 & -0.0928 & 0.8643 & 0.6467 & 1.3085 & 2.3139 & 3.0522 & -0.3979 & -0.1598 \\ 0.9018 & 0.2263 & 1.4657 & 1.4657 & 0.2275 & 0.2356 & -1.4373 & 0.3001 & -4.9956 & -3.1842 & -3.2626 & -0.0159 & 0.0629 \end{bmatrix},$$

$$K_i = 10^{-3} \times \begin{bmatrix} -0.1450 \\ 0.2436 \end{bmatrix}. \tag{34}$$

From Fig. 4, we can observe that the generalized stability diagram of Nyquist for the proposed GWO-tuned LQG servo controller is very close to the actual diagram of the VSP-HVDC model and it illustrates that the proposed controller has approximated the actual VSP-HVDC model accurately. Besides, the performed distance from the critical point, $(-1, 0)$, points to the suitable stability range of these two models (the actual VSP-HVDC model and the proposed GWO-tuned LQG servo controller).

4.2. VSP-HVDC with the proposed LQG strategy

The VSP-HVDC model introduced in Section 2 has been achieved on the basis of the proposed LQG strategy by a Kalman Filter and an LQI tracker, for which the state-space description is presented in Section 3. From the system matrices in the state-space model, the performance of the LQG controller by the proposed tracker can be evaluated. As mentioned in the preceding, the Gaussian probability distribution error, between actual and estimated state variables, is considered for the evaluation of the proposed LQG strategy.

4.2.1. GWO-based tuning for weighting matrices

As explained in Section 3.3, in addition to trial-and-error approach, a systemic approach based on heuristic algorithm is used for a better tuning of weighting matrices of Q_k and R_k in the proposed LQG strategy in order to solve the algebraic Riccati equations and then obtain the optimal feedback gain matrix K. Table 1 shows results of cost function deviations versus iteration in the three performance indices. As it illustrates, the performance index IAE fits more in the proposed GWO-based tuning method, comparing with the performance indices ITAE and ITSE.

Thus finally, the optimal state-feedback gain K which consists of two matrices K_i and K_f to include the dynamics of the integral action and the Kalman Filter can be computed for the VSP-HVDC system equipped with the LQG strategy,

$$K = \begin{bmatrix} -K_f & K_i \end{bmatrix}_{(2 \times 14)},$$

where the obtained values of K_i and K_f matrices from the process in Section 3 are given in (34).

Filter state observer to estimate all the states of the noisy MIMO system. In this section, the performance of the Kalman state observer is studied on the VSP-HVDC model in the presence of noise.

Fig. 5 depicts the variation of actual and estimated frequency deviations in both Area 1 and Area 2 using the proposed LQG strategy for the VSP-HVDC model. The obtained simulation results from the MIMO model considering noise are referred to the "actual" case; the ones from the system in the absence of noise are referred to the "ideal" scenario. As it can be observed from Fig. 5, the proposed LQG servo–controller based on LQI tracker, which has been tuned by using the GWO algorithm, presents accurate and suitable dynamic response in the estimation process. We also provide the digitized results for Figs. 5a and b through Table 2 and Table 3, respectively. The error deviation means the
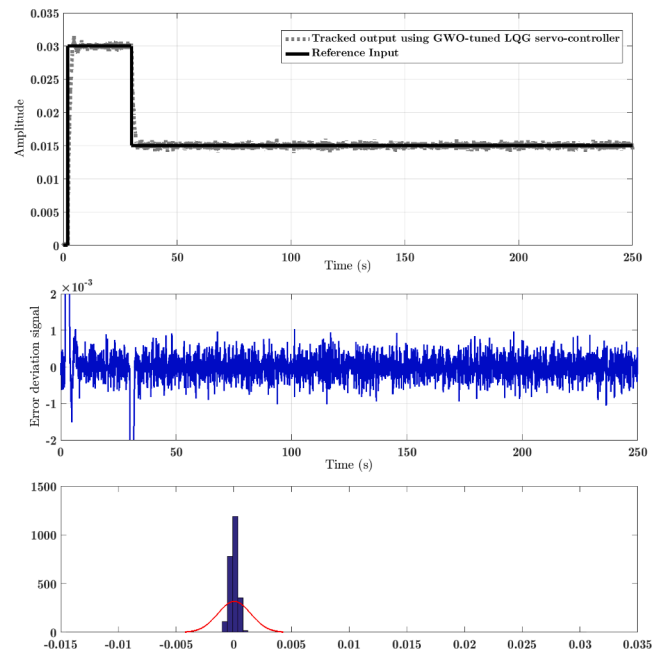

Fig. 6. Evaluation of the proposed LQG servo controller tuned by GWO in the tracking target.

Frequency Deviation $\Delta\omega_1$ (p.u.) in Area 1 for VSP-HVDC Model

AC Power Deviation $\Delta P_{ac,12}$ (p.u. MW) for VSP-HVDC Model

Injected DC Power Deviation $\Delta X_{1,vsp1}$ (p.u. MW) for VSP-HVDC Model
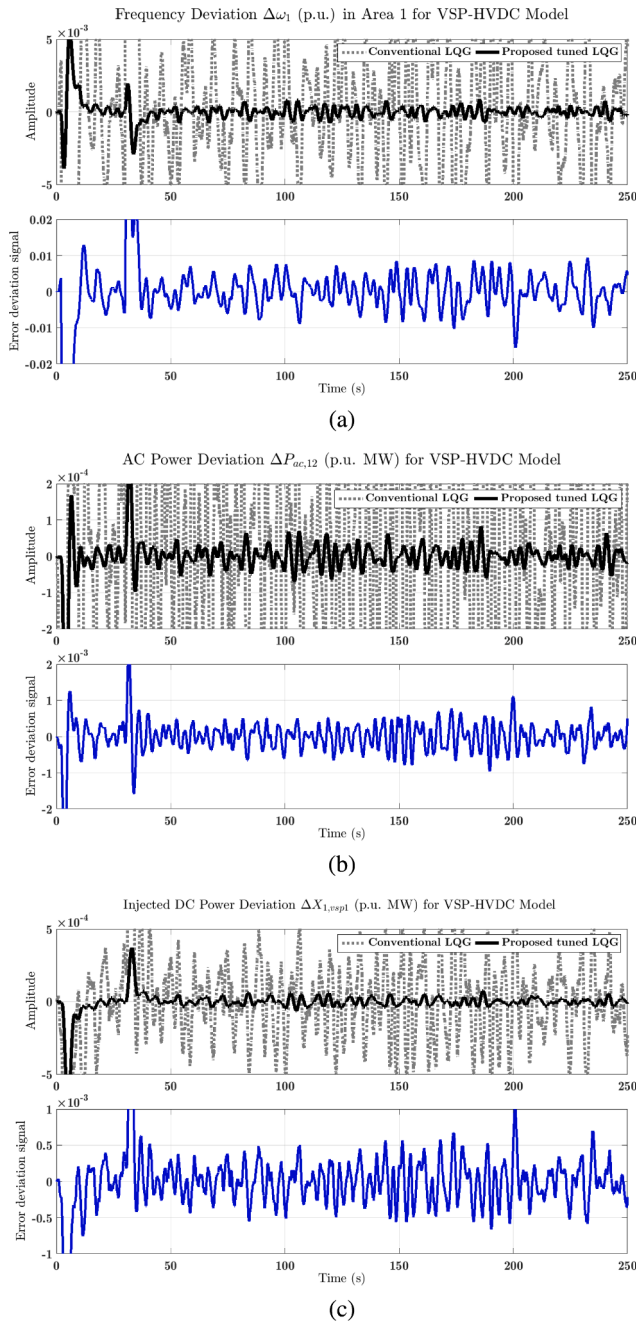

Fig. 7. A comparison of the performance between the conventional LQG regulator and the proposed GWO-tuned LQG servo controller in estimating state variables of frequency and AC/DC power deviations. (a) $\Delta\omega_1$; (b) $\Delta P_{ac,12}$; (c) $\Delta X_{1,vsp1}$.

difference between the actual noisy signal and estimated one. It can be concluded that the estimated variables ($\Delta\omega_1$, $\Delta\omega_2$) have been approximated by the tuned LQG servo controller, after an implementation of noise in the system. The Kalman Filter estimates $\Delta\omega_1$ and $\Delta\omega_1$ with small error in the estimation stage. Besides, the error between the actual frequency deviations and the estimated ones is close to the normal Gaussian probability distribution. Notably, we can see that the estimation on $\Delta\omega_1$ (Fig. 5a) has smaller error overall, comparing with the one
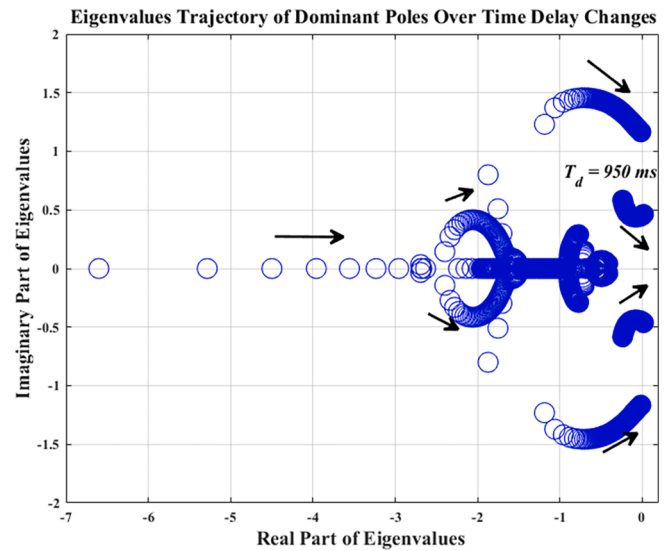
Eigenvalues Trajectory of Dominant Poles Over Time Delay Changes

Fig. 8. Eigenvalue trajectory of dominant poles for the VSP-HVDC model over time delay deviations.

on $\Delta\omega_2$ (Fig. 5b). This is mainly due to the fact that the step-load change fault occurs in Area 1 and the target of the proposed LQG controller design has been centralized on Area 1.

In Appendix A, we provide the simulation results for the estimation targets on the AC power flow deviation ($\Delta P_{ac,12}$) between these two areas, the injected DC power deviations ($\Delta X_{1,vsp1}$, $\Delta X_{1,vsp2}$) and their derivative terms ($\Delta X_{2,vsp1}$, $\Delta X_{2,vsp2}$) from the VSP-based HVDC link. The results also validate the effectiveness of the Kalman Filter within the proposed LQG servo controller tuned by the GWO algorithm in estimating these variables. From the index of error deviation, one can observe that the performance of the proposed LQG controller in estimation process of the state variables corresponding to AC/DC power flows is even better than the one in estimating frequency state variables. The Gaussian probability distribution of the error between the actual states and the estimated ones also indicate meticulous accuracy of the estimation target.

4.2.3. Simulation results of the tracking target

The proposed LQG servo controller tuned by GWO is also supposed to guarantee an appropriate reference signal pursuit in the closed-loop system. An integral action in the LQI is added to the LQG controller to realize the tracking target. Next, we show the simulation results of the tracking performance. Note that for the global closed-loop system in Fig. 3, the inputs become the reference signal *r*. Thus correspondingly we let *r* be the step load changes in (33) as the "new" system inputs. The evaluation of the proposed GWO-tuned LQG controller using an LQI in the tracking target is presented in Fig. 6.

From Fig. 6 we can see that, the LQI part could keep the output tracking the reference command *r* in the proposed LQG servo controller for the VSP-HVDC system in the presence of noise. Besides, by applying this controller, the error deviation signal between the output and the reference command of the global closed-loop system is close to zero. To conclude, the proposed LQG controller tuned by the GWO algorithm for the VSP-HVDC system which may consist of process disturbances and measurement noise can achieve both targets on state estimation and reference tracking.

4.2.4. Comparisons: proposed LQG servo controller vs conventional regulator

This subsection focuses on comparative results between our optimized LQG servo–controller using GWO with added LQI tracker versus the conventional LQG regulator which does not have reference tracking functionality, as described in Section 3.1. With the explanations and the results in the preceding, we can have a comparison between these two controllers in the same simulation scenarios where fault signals, process disturbances and measurement noise are included.

Fig. 7 provides simulation results for comparisons between the proposed GWO-tuned LQG controller and the conventional one in estimating state variables of frequency and AC/DC power deviations. It can be seen that the proposed GWO-tuned LQG servo–controller estimates more accurate in these scenarios, comparing with the conventional LQG regulator whose estimations in these state variables have large deviations from the actual ones. To be mentioned till this end, in Fig. 5, we "zoom in" to see how the proposed LQG controller can have meticulous accuracy of the estimation target, while in Fig. 7 we keep the original size and observe that the conventional LQG regulator has a much worse performance in estimating the state variables.

4.3. Discussions

In this part, we provide a short discussion on possible effects from the communication delay. Since the main focus of this paper is on control strategy for a stabilization and dynamic improvement of the VSP-HVDC system especially in the scenario where there exists noise, the communication network for the data exchange is assumed to be ideal in the most scenarios of this paper. However, the topic of communication delay related to a controller is still of high importance and great practical relevance. Let us consider the scenario where the communication delay would appear in the AGC loop of Eqs. (9)–(12) in Section 2.1, due to the restriction and expansion of the two-area system with a long distance HVDC link [27]. The system model with communication delays on the AGC can still be derived in the form of (17), by modeling the delay block through the first–order Pade approximation; we refer to [28] for this technique.

Fig. 8 shows the eigenvalue trajectory of dominant poles for the studied VSP-HVDC model over time delay deviations. According to the obtained simulation results, the termination criteria happens in $T_d = 0.95$ seconds or 950 ms. On the other hand, the maximum performed delay on the system model for which the real part of eigenvalues stays on non–positive values, will be about 950 ms. The VSP-HVDC system will have instability problems when the communication delay exceeds this limit. In general, this margin of 950 ms is still enough since in real practice considering advanced communication technologies like PMUs (Phasor Measurement Units) the communication delays are much less than this value.

5. Conclusion

The concept of VSP-based virtual inertia emulation in AC/DC interconnected system has been discussed and presented in this paper. Till this end, in order to achieve the estimation and tracking targets, a proposed LQG servo controller using an LQI tracker and the GWO algorithm for the tuning of the weighting matrices has been designed for a novel high-level control application of the VSP–HVDC system which may consist of noise. According to the obtained results, we can have the following remarks:

(i) To achieve the system analysis on the studied VSP-HVDC model equipped with proposed LQG servo controller, Nyquist's stability criterion method was used. From the obtained Nyquist diagram, it's feasible to conclude that the proposed LQG servo controller could present acceptable and stable performance, and it can also estimate the state variables of the VSP–HVDC model with small possible error.

(ii) The first simulation was performed to validate the proposed GWO-tuned LQG controller on the estimation target. Variations of the state variables $x_1, x_2, x_9, x_{10}, x_{11}, x_{12}, x_{13}$ as $\Delta\omega_1, \Delta\omega_2, \Delta P_{ac,12}, \Delta X_{1,vsp1}, \Delta X_{2,vsp1}, \Delta X_{1,vsp2}, \Delta X_{2,vsp2}$ were studied. In the simulation results, the Gaussian probability distribution error, between the actual state variables and the estimated state ones, was presented for the evaluation of the Kalman Filter state estimator. It can be seen that, all the obtained results have emphasized a good performance of the proposed LQG controller.

(iii) The second simulation results have been applied for the evaluation of the tracking target which is based on an LQI strategy in the proposed LQG controller. As illustrated in the results, the LQI tracker could keep the output *y* tracking the input reference signal *r*. Besides, by applying this tracker, the error deviation signal for the difference of *y* and *r* is close to zero.

(iv) In the end, we perform a comparison study between our proposed GWO-tuned LQG controller and the conventional LQG regulator (which does not have the reference tracking capability). The simulation results have indicated that the proposed LQG controller tuned by GWO can have a more accurate estimation of the state variables, while the conventional one fails to have large deviations between its estimated states and the actual ones. From the other perspective, it also validate the effectiveness of the proposed LQG controller for a novel application on the VSP-HVDC system considering the presence of noise.

CRediT authorship contribution statement

Elyas Rakhshani: Conceptualization, Methodology, Software, Resources. **Iman Mohammad Hosseini Naveh:** Data curation, Formal analysis, Visualization, Writing - original draft. **Hasan Mehrjerdi:** Supervision, Software. **Kaikai Pan:** Conceptualization, Formal analysis, Investigation, Writing - original draft, Writing - review & editing.

Declaration of Competing Interest

The authors declare that they have no known competing financial interests or personal relationships that could have appeared to influence the work reported in this paper.
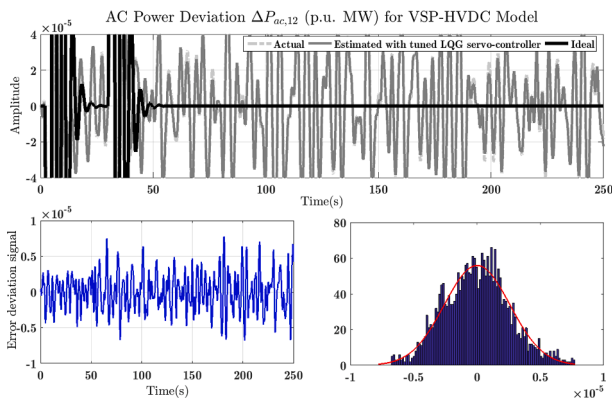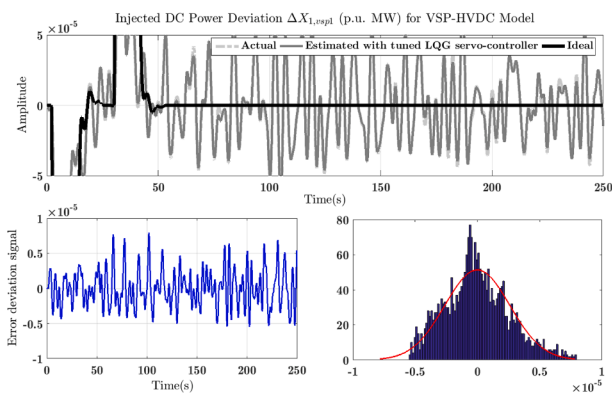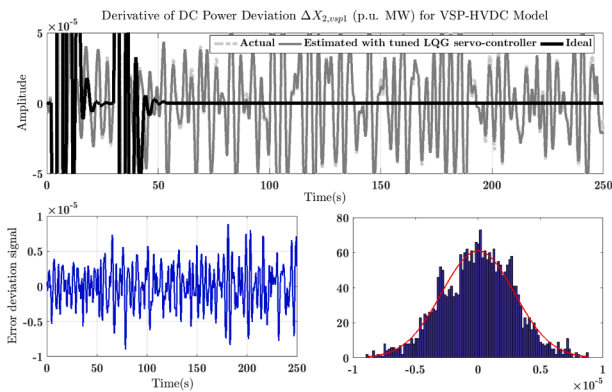
Appendix A

We present the simulation results in the estimation target of the proposed LQG servo controller. The results in estimating state variables $\Delta P_{ac,12}, \Delta X_{1,vsp1}, \Delta X_{2,vsp1}, \Delta X_{1,vsp2}, \Delta X_{2,vsp2}$ are shown in Fig. 9, Fig. 10 and Fig. 11.

Fig. 9. Variation of actual and estimated tie-line AC power using the proposed LQG controller tuned by GWO.

(a)

(b)

Fig. 10. Variation of actual and estimated injected DC power and its derivative in VSP of Area 1 using the proposed LQG controller tuned by GWO. (a) $\Delta X_{1,vsp1}$; (b) $\Delta X_{2,vsp1}$.

(a)

(b)

Fig. 11. Variation of actual and estimated injected DC power and its derivative in VSP of Area 2 using the proposed LQG controller tuned by GWO. (a) $\Delta X_{1,vsp2}$; (b) $\Delta X_{2,vsp2}$.

Appendix B. Supplementary material

Supplementary data associated with this article can be found, in the online version, at https://doi.org/10.1016/j.ijepes.2020.106752.

References

[1] Kundur P, Paserba J, Ajjarapu V, Andersson G, Bose A, Canizares C, et al. Definition and classification of power system stability IEEE/cigre joint task force on stability terms and definitions. IEEE Trans Power Syst 2004;19:1387–401.

[2] Tielens P, Hertem DV. The relevance of inertia in power systems. Renew Sustain Energy Rev 2016;55:999–1009.

[3] Rakhshani E, Sadeh J. Practical viewpoints on load frequency control problem in a deregulated power system. Energ Convers Manage 2010;51:1148–56.

[4] Rakhshani E, Rodriguez P. Inertia emulation in AC/DC interconnected power systems using derivative technique considering frequency measurement effects. IEEE Trans Power Syst 2017;32:3338–51.

[5] Eriksson R, Modig N, Elkington K. Synthetic inertia versus fast frequency response: a definition. IET Renew Power Gener 2018;12:507–14.

[6] Dreidy M, Mokhlis H, Mekhilef S. Inertia response and frequency control techniques for renewable energy sources: A review. Renew Sustain Energy Rev 2017;69:144–55.

[7] Hafiz F, Abdennour A. Optimal use of kinetic energy for the inertial support from variable speed wind turbines. Renew Energy 2015;80:629–43.

[8] Gonzalez-Longatt FM. Effects of the synthetic inertia from wind power on the total system inertia: simulation study. In: Proc. 2nd Int. Symp. Environ. Friendly Energies Appl. IEEE; 2012. https://doi.org/10.1109/efea.2012.6294049.

[9] Driesen J, Visscher K. Virtual synchronous generators. In: Proc. IEEE Power & Energy Soc. General Meeting. IEEE; 2008. https://doi.org/10.1109/pes.2008.4596800.

[10] Castro LM, Acha E. On the provision of frequency regulation in low inertia AC grids using HVDC systems. IEEE Trans Smart Grid 2016;7:2680–90.

[11] Guan M, Pan W, Zhang J, Hao Q, Cheng J, Zheng X. Synchronous generator emulation control strategy for voltage source converter (VSC) stations. IEEE Trans Power Syst 2015;30:3093–101.

[12] Alipoor J, Miura Y, Ise T. Power system stabilization using virtual synchronous generator with alternating moment of inertia. IEEE J Emerg Sel Top Power Electron 2015;3:451–8.

[13] Rakhshani E, Torres JLR, Palensky P, der van Meijden M. Determination of maximum wind power penetration considering wind turbine fast frequency response. In: Proc. IEEE PowerTech Conf. IEEE; 2019. https://doi.org/10.1109/ptc.2019.8810492.

[14] Rakhshani E, Rodriguez P, Cantarellas AM, Remon D. Analysis of derivative control based virtual inertia in multi-area high-voltage direct current interconnected power systems. IET Gener Transm Distrib 2016;10:1458–69.

[15] Zhu J, Booth CD, Hung W, Guerrero JM, Adam GP. Generic inertia emulation controller for multi-terminal voltage-source-converter high voltage direct current systems. IET Renew Power Gener 2014;8:740–8.

[16] Pan K, Rakhshani E, Palensky P. False data injection attacks on hybrid AC/HVDC interconnected systems with virtual inertia–vulnerability, impact and detection. IEEE Access 2020;8:141932–45.

[17] Bevrani H, Ise T, Miura Y. Virtual synchronous generators: A survey and new perspectives. Int J Electr Power Energy Syst 2014;54:244–54.

[18] Rakhshani E, Remon D, Cantarellas AM, Garcia JM, Rodriguez P. Virtual synchronous power strategy for multiple HVDC interconnections of multi-area AGC power systems. IEEE Trans Power Syst 2017;32:1665–77.

[19] Rodriguez P, Candela I, Luna A. Control of PV generation systems using the synchronous power controller. In: Proc. IEEE Energy Conversion Congress and Exposition. IEEE; 2013. https://doi.org/10.1109/ecce.2013.6646811.

[20] Zhang M, Sun P, Cao R, Zhu J. LQG/LTR flight controller optimal design based on differential evolution algorithm. In: Proc. Int. Conf. Intelligent Computation Technology and Automation. IEEE; 2010. https://doi.org/10.1109/icicta.2010.302.

[21] Rakhshani E, Remon D, Cantarellas A, Garcia JM, Rodriguez P. Modeling and sensitivity analyses of VSP based virtual inertia controller in interconnected power systems. Elect Power Energy Syst 2016;141:246–63.

[22] Hespanha JP. Lecture notes on lqr/lqg controller design. Knowledge Creation Diffusion Utilizat. 2005.

[23] Ostertag E. Mono- and Multivariable Control and Estimation. Berlin Heidelberg: Springer; 2011. https://doi.org/10.1007/978-3-642-13734-1.

[24] Mirjalili S, Mirjalili SM, Lewis A. Grey wolf optimizer. Adv Eng Softw 2014;69:46–61.

[25] Skogestad S, Postlethwaite I. Multivariable feedback control. In: Advances in Industrial Control. Verlag: Springer; 1996. p. 559. https://doi.org/10.1007/1-84628-092-3_5.

[26] Johansson KH. Interaction bounds in multivariable control systems. Automatica 2002;38:1045–51.

[27] Rakhshani E, Remon D, Rodriguez P. Effects of pll and frequency measurements on lfc problem in multi-area hvdc interconnected systems. Int J Electr Power Energy Syst 2016;81:140–52.

[28] Silva GJ, Datta A, Bhattacharyya SP. PID controllers for time-delay systems. Springer Science & Business Media; 2007.